



Provenance of sediments in the Zhongnan Seamount, South China Sea since MIS 3: Insights from clay minerals and geochemical signatures

Letian Zeng ^{a,b,c}, Ce Wang ^{a,b,c,*} , Ming Su ^{a,b,c}, Heqi Cui ^{a,b,c}

^a School of Marine Sciences, Sun Yat-sen University, Zhuhai, 519082, China

^b Southern Marine Science and Engineering Guangdong Laboratory (Zhuhai), Zhuhai, 519082, China

^c Guangdong Provincial Key Laboratory of Marine Resources and Coastal Engineering, Zhuhai, 519082, China

ARTICLE INFO

Handling editor: I Hendy

Keywords:

Provenance
Sediments
Clay minerals
Geochemistry
Zhongnan seamount
South China Sea

ABSTRACT

As the widespread and prominent features of the ocean, seamounts are served as natural repositories for sediments, creating a special environment for understanding the sediments from terrigenous source to oceanic sink. However, opportunities to delve into the provenance and sedimentary processes of seamounts has been notably restricted. Here we examine the geochemistry and clay minerals of sediments from the Zhongnan Seamount in the South China Sea, with aims to reveal the provenance of sediments and investigate the transport pathways during the glacial-interglacial periods. Geochemical results indicate that the parent rocks of the sediments vary from andesite and felsic volcanic rocks, which were formed under tectonic settings similar to the continental island arc, suggesting a predominantly terrigenous source. Provenance results indicate that the sediments of the seamount were primarily derived from the islands of Taiwan Island, Luzon, and the Red River, with the sources of sediments varied during glacial-interglacial periods. Since MIS 3, shifts in the provenance of seamount sediments have been associated with variations in sea level prompted by climate change and the transport dynamics of ocean currents. This study proposes the potential of sediments in seamounts to record the hydrodynamic patterns and reveal transport pathways in the source-to-sink systems.

1. Introduction

Detrital sediments derived from continents are primarily transported to oceans through three agents: rivers, winds, and glaciers (Hay, 1998). Once entering the ocean, the sediments are strongly affected by hydrodynamic processes during their trip to depositional destination (Milliman and Farnsworth, 2011). In the modern age, the direction and velocity of ocean currents in different layers can be precisely decoded through observations of physical oceanography (Wang et al., 2011; Zhu et al., 2019). However, such methods are unable to record the hydrodynamic conditions of ancient time. Ocean currents serve as mediums for sediment transport, in turn, the sediments that have already deposited can held the ability as indicators for inferring the past ocean currents.

In addition to the ocean currents, topography also plays a significant role in controlling the sediment transport of detritus in the ocean (Liu et al., 2016; Zhong et al., 2017). The ubiquitous seamounts developed in ocean basins act as barriers, altering the velocity and direction of hydrodynamic condition locally and globally, and thus being able to

change the transport processes (Lavelle and Mohn, 2010; Jiang et al., 2021). Additionally, seamounts themselves are natural incubators for organisms and reservoirs for sediments deposition, creating unique biological and sedimentological environments (Turnewitsch et al., 2013). These environmental elements interact with each other, as the hydrodynamic flow patterns carry varying compositions of organic materials and sediments (Clark et al., 2010). As seamounts are widespread and prominent features of the ocean, it is vital to investigate their sediments composition, hydrodynamic condition, and response to climate change (McClain, 2007; Clark et al., 2010; Chen et al., 2021).

Situated at the conjunction of the Eurasian, Indo-Australia and Pacific plates, the South China Sea (SCS) (Fig. 1A) has nearly experienced a complete Wilson cycle, from continental breakup to seafloor subduction, and developed several seamounts nearly along the mid-ocean ridge line. Owing to its specific location, the SCS has also suffered from the East Asian Monsoon (EAM), which frequently intensifies the land-ocean interactions, resulting in the receipt of more than 700 million Mt/y fluvial sediments (Liu and Stattegger, 2014). These features make it possible to provide sufficient sediments for transportation to the open ocean,

* Corresponding author. School of Marine Sciences, Sun Yat-sen University, Zhuhai, 519082, China.

E-mail address: wangce@mail.sysu.edu.cn (C. Wang).

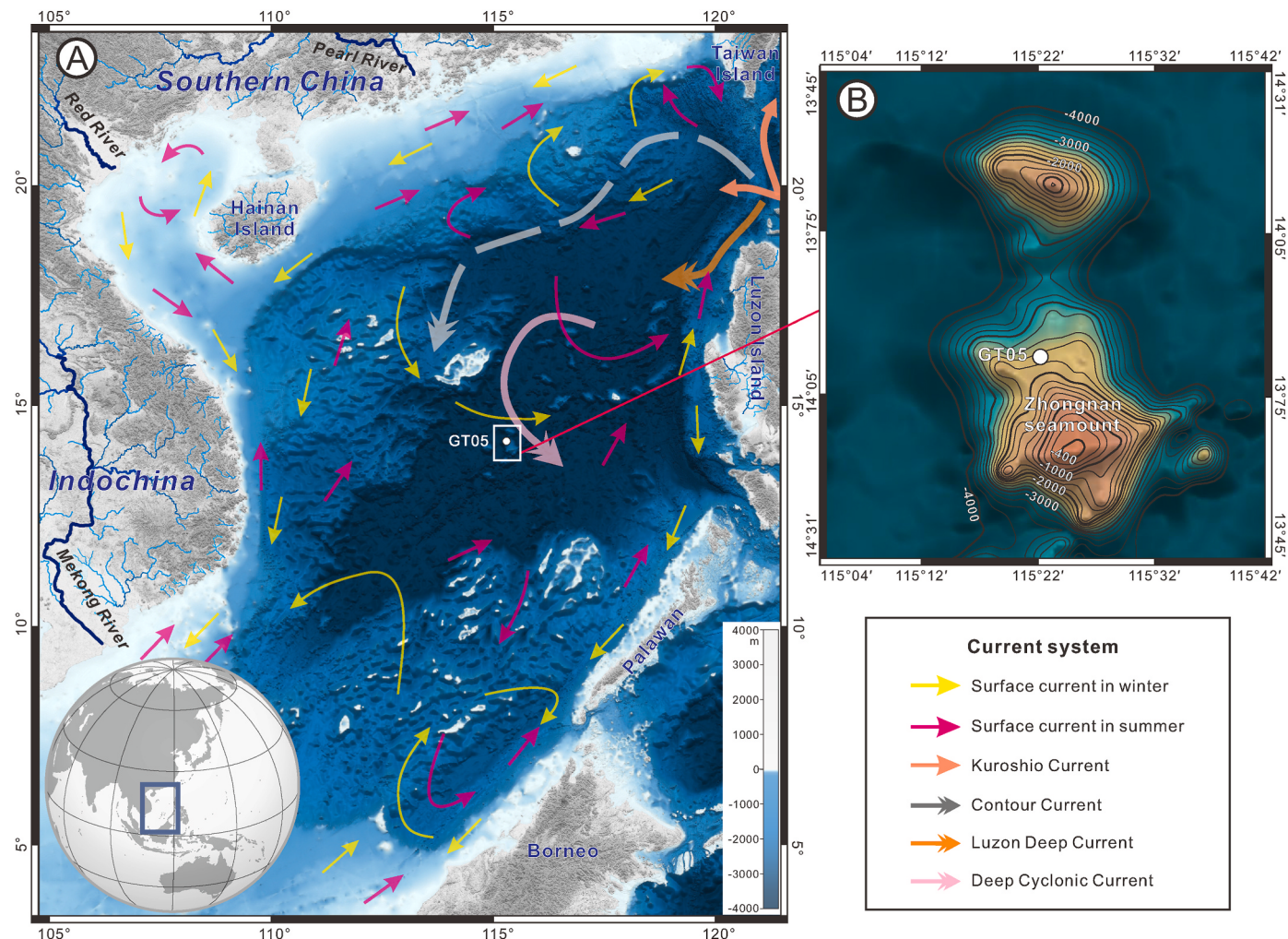


Fig. 1. Topographic map of the South China Sea showing the oceanography and location of GT05 in the Zhongnan seamount, South China Sea. (A) Current systems in the South China Sea. (B) Topography of the Zhongnan Seamount. Surface currents in summer and winter after Wu et al. (2008) and Zhu et al. (2019); Kuroshio Current after Caruso et al. (2006), Nan et al. (2011) and Nan et al. (2015); Deep Water Current after Qu et al. (2006), Wang et al. (2011) and Zhao et al. (2014).

thereby forming the SCS into a natural laboratory for studying the past lives of ocean sediments.

Terrigenous sediments, detached from their parent rocks, are formed under various environmental conditions, including diverse climates and tectonic settings in the adjacent source areas (Liu et al., 2016). The geochemical composition of these sediments yields abundant information about their source rocks, tectonic settings, and climate history (Liu et al., 2009; Hu et al., 2012; Clift, 2016), forming the basis for decoding the sediments provenance, climate evolution, and oceanic conditions (Chen et al., 2021). Geochemistry and clay minerals in the sediments of the SCS are sensitive indicators of climate change, offers a valid approach to deciphering their provenance, transporting pathways, and responses to the climate fluctuations (Liu et al., 2010, 2012). Previous studies have dedicated considerable effort to analyzing the clay minerals and geochemistry of the SCS and its surrounding source terrains (Boulay et al., 2005; Liu et al., 2016; Huang et al., 2021), especially focusing on the sediments from the continental shelf and drainage systems, providing robust datasets for identifying the potential sources of sediments in seamount of the SCS.

Seamounts are common features on the southwest sub-basin (SWSB) of the SCS, among which the Zhongnan seamount is the most typical (Fig. 1A). In this study, core samples were collected from the Zhongnan Seamount in the central SCS for geochemistry and clay minerals analysis. Our study aims to decipher the sediment provenance, evaluate the

hydrodynamic patterns in the deep sea, and reveal the transport pathway of sediments during the late Quaternary glacial-cyclic period.

2. Background

2.1. Geological setting

As the largest marginal sea in the western Pacific, the SCS is bordered by southeastern Eurasian Continent and several islands with China to the north, Indochina to the west, Borneo and Palawan to the south, and Luzon to the east (Fig. 1A). The opening of the SCS started when seafloor spread in the early Oligocene (Taylor and Hayes, 1980, 1983; Brais et al., 1993) and IODP Expedition 367 & 368 found it earlier at ca. 34 Ma (Huang et al., 2019). The evolution of the SCS followed by two NW-SE extension during the late Oligocene and early to middle Miocene in the east sub-basin (ESB) and southwest sub-basin (SWSB) (Li et al., 2014; Sibuet et al., 2016). Previous study suggests that the SWSB and ESB terminated at 16 Ma and 15 Ma, respectively (Li et al., 2014). In addition, after the termination of seafloor spreading, the SCS experienced post-spreading intraplate volcanism (Yan et al., 2014; Ding et al., 2016), forming widespread volcanic seamount chains in the sub-basins after the cessation of seafloor spreading (Yan et al., 2008). The subduction and magmatic activities influenced the present pattern of the SCS (Sibuet et al., 2016).

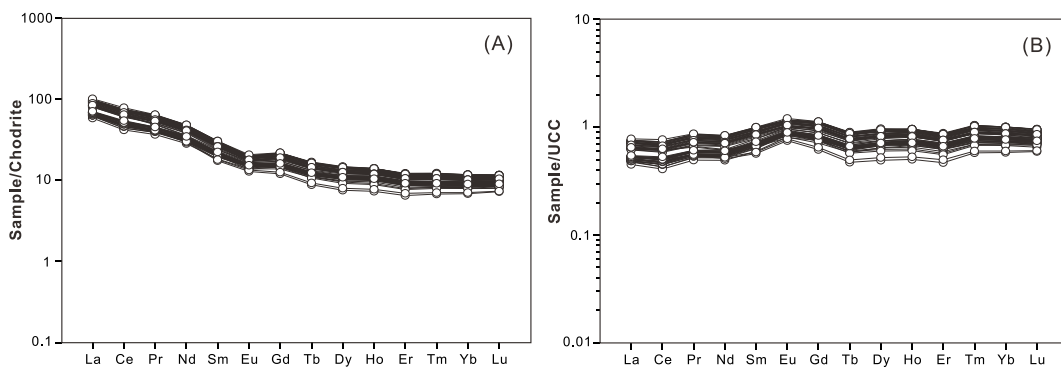


Fig. 2. (A) Chondrite normalized REE plot of sediments in core GT05. (B) UCC normalized REE plot of sediments from core GT05. Chondrite data are adopted from Sun and McDonough (1989). UCC data are collected from Rudnick and Gao (2003).

The SWSB is a V-shape sub-basin featuring a NE-SW trend fossil spreading ridge, and most of the seamounts develop in the northeastern section (Zhang et al., 2020a). The Zhongnan Seamount, located in the northeast of the SWSB, is a relatively larger member of the SWSB seamounts chain (Fig. 1A). The Zhongnan Seamount possess an approximately 3600 m straight height from bottom to top, and its northern slope is much lower than the southern (Fig. 1B). Previous study has dated the age of alkali basalt collected from the northern slope of Zhongnan Seamount, yielding an Ar-Ar age of 6.64 ± 0.42 Ma (Yan et al., 2014).

2.2. Climatic condition

As the most important component of East Asia's climate system, the EAM is well developed due to the distinct thermodynamic properties of the largest continent (Eurasia), the widest open oceans (Pacific), and the world's highest plateau (Tibetan Plateau) (Huang et al., 2003; Li et al., 2016). Consisting of two types of monsoons, the EAM generates strong southerly winds carrying warm and wet air from the ocean to the land (East Asian Summer Monsoon, EASM). This process is accompanied by continental heating, which leads to the development of low pressure over central China mainland. In contrast, the EAM is characterized by enhanced northerly winds with cold and dry air from the land to the ocean during the East Asian Winter Monsoon (EAWM), resulting from continental cooling and the development of high pressure over northern Asia (Webster, 1994; Wang et al., 2006; Huang et al., 2012). The alternating summer and winter monsoon create seasonal precipitation patterns, which in turn lead to variations in river runoff and chemical weathering of rocks.

The influence of the monsoon varies considerably under different climatic conditions, especially during the glacial-interglacial cycles. During the late Quaternary period, the EAWM intensified in the glacial ages, while the EASM strengthened in interglacial ages (Wang et al., 1999; Jian et al., 2001; Sun et al., 2006). Consequently, intense physical denudation may have occurred frequently on land as intensified the EAWM during the glacial ages (Liu et al., 2016), whereas rainfall, river runoff, and chemical weathering would have increased in surrounding drainage systems as the EASM was strengthened during interglacial periods (Wang et al., 1999; Tamburini et al., 2003).

2.3. Oceanography

Surface ocean currents in the SCS exhibit seasonal variations (Fig. 1A), consisting of two different circulation systems triggered by the EASM and EAWM, respectively (Gan et al., 2006; Liu et al., 2008a). Additionally, the Kuroshio Current, invaded from the Luzon Strait, yields a crucial effect on the upper layer of the SCS (Hu et al., 2000; Nan et al., 2011, 2015). The intermediate layer circulations in the SCS are similar to those in upper layers (Isobe and Namba, 2001), but significantly affected by the mesoscale eddies originating from intrusion of the

Kuroshio Current (Zhang et al., 2014). Deep ocean currents in the SCS are driven by water exchange between the Pacific Ocean and the SCS, with the intrusion of the North Pacific Deep Water (NPDW) via the Luzon Strait (Qu et al., 2006; Lan et al., 2013; Zhao et al., 2014). The cyclonic deep circulation is formed due to the dissipation of the high potential vorticity (Lan et al., 2013; Zhu et al., 2017).

The SCS has been greatly affected by the glacial-interglacial cycles during the late Quaternary, as the exact opposite variations have altered greatly in climatic and oceanographic condition (Wang and Sun, 1994; Tamburini et al., 2003; Liu et al., 2016; Zhao et al., 2023). During glacial-interglacial cycles, global sea levels rise or fall in response to the climate change, with sea levels dropped more than 120 m compared to the present level during glacial ages (Lambeck et al., 2014; Miller et al., 2020). Consequently, the continental shelf in the SCS was exposed, resulting in the seaward extension of rivers, erosion of deposited strata in continental shelf, and alterations in ocean currents from the surface to deep layers (Wang and Sun, 1994; Broecker et al., 2008; Chen et al., 2017; Zhao et al., 2023).

3. Samples and methods

Sediment gravity core GT05 (122 cm), retrieved from the northern slope of Zhongnan Seamount (14.1069° N, 115.3794° E, with a water depth of 2465 m), was collected specifically for the analysis of trace elements and clay minerals. The calibrated age model, obtained through Accelerated Mass Spectrometry (AMS) ^{14}C isotope dating, is derived from Wang et al. (2025). The results indicate that core GT05 spans three Marine Isotope Stages (MIS) from middle MIS 3 to MIS 1.

3.1. Trace elements

A total of 56 sediment samples spaced 2 cm interval were collected for trace elements analysis, which were conducted on Elan DRC-e ICP-MS. The detailed sample-digesting procedure was as follows: (1) Sample powder (200 mesh) were placed in an oven at 105°C for drying, carbonate and organic matter were removed by HNO_3 and H_2O_2 respectively; (2) sample powder was placed in an Teflon bomb and digested by HNO_3 , HF and HClO_4 (all of the agent are ultrapure grade) in an oven at 190°C ; (3) After cooling, the final solution was transferred to a 100 ml polyethylene bottle, add 1 ml (Rh + Re) mixed standard solution (1 mg/L), and then diluted to 100 g by the addition of Milli-Q water. The analytical precision and accuracy are same as Liu et al. (2008b) while standard samples GBW07316, BHVO-2 and BCR-2 were used in the experiment. The results are presented in Supplementary Table 1.

3.2. Clay mineral

A total of 52 sediment samples were chosen for clay minerals analysis, which were tested through X-ray diffraction (XRD) with Cu target

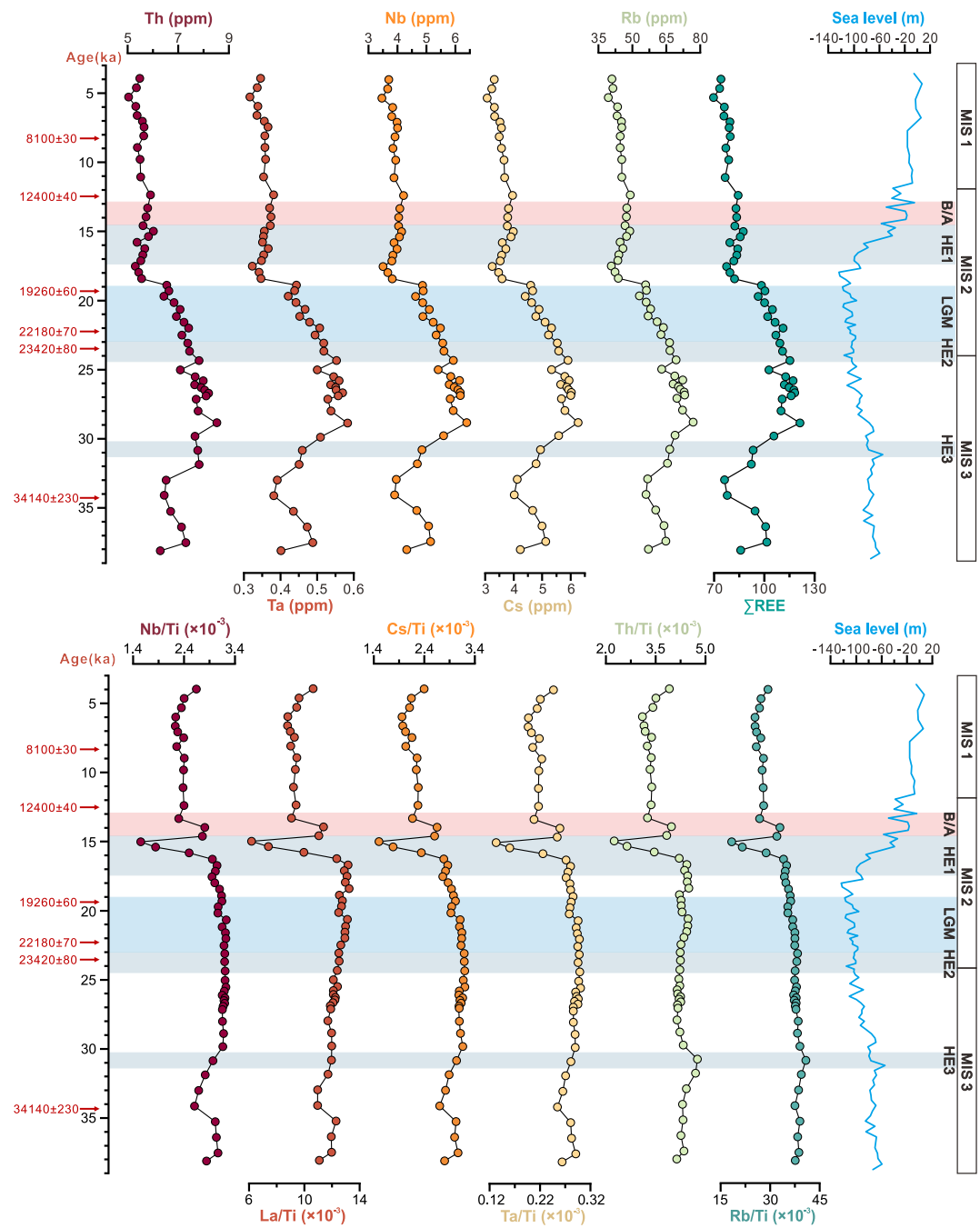


Fig. 3. Trace element variations of sediments in core GT05 since 38 ka BP. B/A: Bølling/Allerød event; LGM: Last Glacial Maximum; HE1: Heinrich event 1; HE2: Heinrich event 2; HE3: Heinrich event 3. The data of sea level are adopted from Miller et al. (2020).

in D-MAX Rapid II diffractometer at the State Key Laboratory for Mineral Deposits Research, Nanjing University. Clay minerals were extracted by centrifugal method, air-drying and ethylene-glycol directional sheet were made before XRD running. The scan range is from 3 to 36° with step of 0.01. The relative proportions of the four clay minerals were calculated from peak areas, and their identification was based on characteristic basal spacings: smectite (15–17 Å), illite (10 Å), and kaolinite/chlorite (7 Å), using Jade 6.5 software. The relative proportions of kaolinite and chlorite were further distinguished using their 3.57 Å and 3.54 Å reflections, respectively. The weighting factor in Biscaye (1965) is not used in this article. Besides, the illite chemistry index is estimated using the ratio of 5 Å and 10 Å illite peaks (Ehrmann, 1998). The result is presented in Supplementary Table 2.

4. Results

4.1. Trace elements and REE

Chondrite-normalized Rare Earth Element (REE) patterns show apparent fractionation between light REE (LREE) and heavy REE (HREE), with the ratio of LREE to HREE ranges from 6.06 to 8.94 (Supplementary Table 1). This indicates a slight LREE enrichment and smooth HREE slopes of the sediments in core GT05 (Fig. 2A). Slightly negative Eu anomalies ($\text{Eu}/\text{Eu}^* = 0.79\text{--}0.89$) are observed in core GT05, consistent with the chondrite-normalized REE patterns (Fig. 2A). Samples characterized by $(\text{La}/\text{Yb})_n$ values (6.36–10.30) and $(\text{La}/\text{Sm})_n$ values (2.93–4.01) imply a prominent fractionation between LREE and HREE (Supplementary Table 2). Upper continental crust (UCC)-normalized

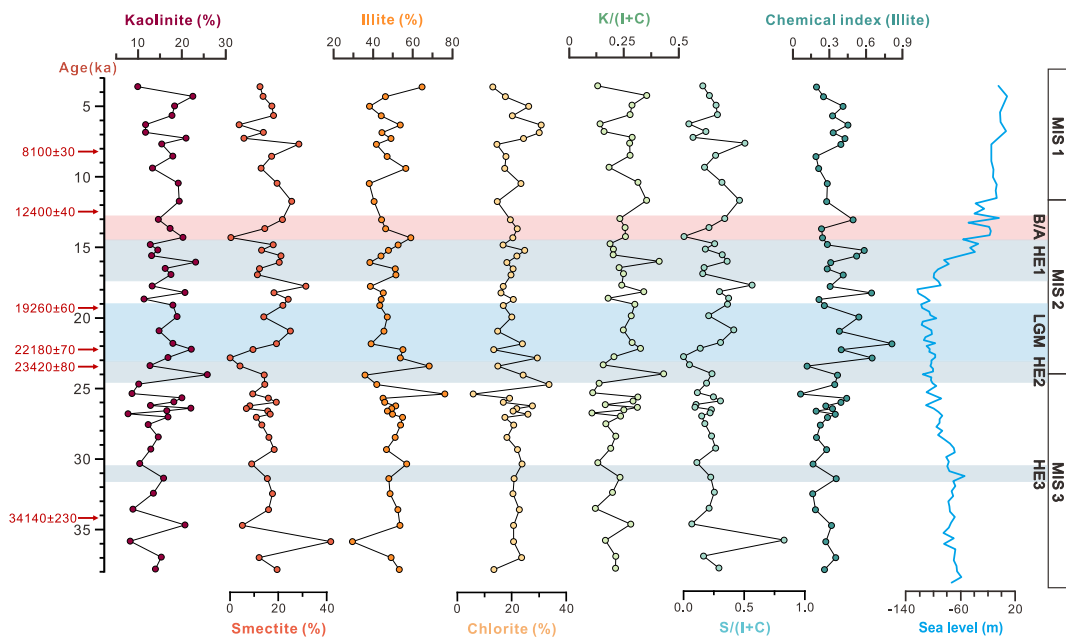


Fig. 4. Clay mineralogy variations of sediment in core GT05 since 38 ka BP. K/(I + C): Kaolinite/(Illite + Chlorite); S/(I + C): Smectite/(Illite + Chlorite).

REE patterns display similarities between these sediments and UCC, with most samples clustering around 1, although some values are relatively low (Fig. 2B).

Trace elements variations of sediments in core GT05 since 38 ka BP are shown in Fig. 3, we found that single elements show relatively high values from HE3 to LGM, there is a sudden lowering at the end of LGM and become stable at relatively lower values. Besides, Ti-normalized ratios show relatively high values before B/A, however, there is a sever variation (drop and rise) before B/A, then become stable at lower values after B/A (Fig. 3). We found a great response between elements and climate events and grouped the sediments in the later analysis, in order to better discover the trigger causing the variations.

4.2. Clay mineralogy

The clay mineral assemblages of core GT05 can be divided into three main groups chronologically from MIS 3 to MIS 1 (Supplementary Table 2). In MIS 3, illite (30–76 %, average 50 %) and chlorite (6–34 %, average 21 %) are relatively high, while kaolinite ranges from 9 % to 22 % (average 14 %). Additionally, all but one of the smectite values are abnormally high, ranging from 5 % to 19 % (average 15 %). Clay minerals in MIS 2 mainly consist of illite (36–68 %, average 48 %) with

relatively small proportion of chlorite (15–24 %, average 20 %) and kaolinite (11–26 %, average 17 %), and smectite fluctuates greatly (0–31 %, average 16 %). Similarly, in MIS 1, illite remains predominant (38–65 %, average 47 %), accompanied by relatively high percentages of chlorite (13–31 %, average 20 %), kaolinite (10–23 %, average 17 %), and smectite (4–28 %, average 16 %).

Clay minerals in core GT05 are dominated by illite but show a decrease over time. In contrast, smectite exhibits an increase from MIS 3 to MIS 2 (Fig. 4). However, chlorite and kaolinite show the opposite fluctuations: chlorite decreases in MIS 2 then increase in MIS 1, while kaolinite increases during MIS 2 and decreases slightly in MIS 1 (Fig. 4). In addition, the illite chemical index crystallinity is highest during MIS 2, ranging from 0.12 to 0.82 (average 0.4) (Fig. 4).

5. Discussion

5.1. Geochemical characteristics of sediments

Seamounts grow from the seafloor mainly through volcanism, forming a basement consisting of pillow lavas and a small amount of volcanic clastic rocks (Staudigel and Koppers, 2015). Since seamounts can produce detritus through weathering of themselves, it is essential to

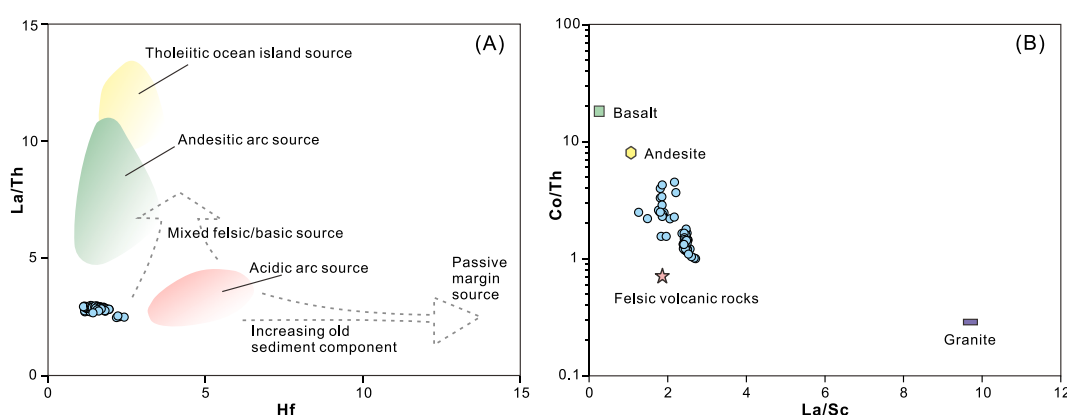


Fig. 5. Discrimination plots show the parent rocks of sediments in core GT05. (A) Hf vs. La/Th (Floyd and Leveridge, 1987). (B) La/Sc vs. Co/Th (Wronkiewicz and Condé, 1987).

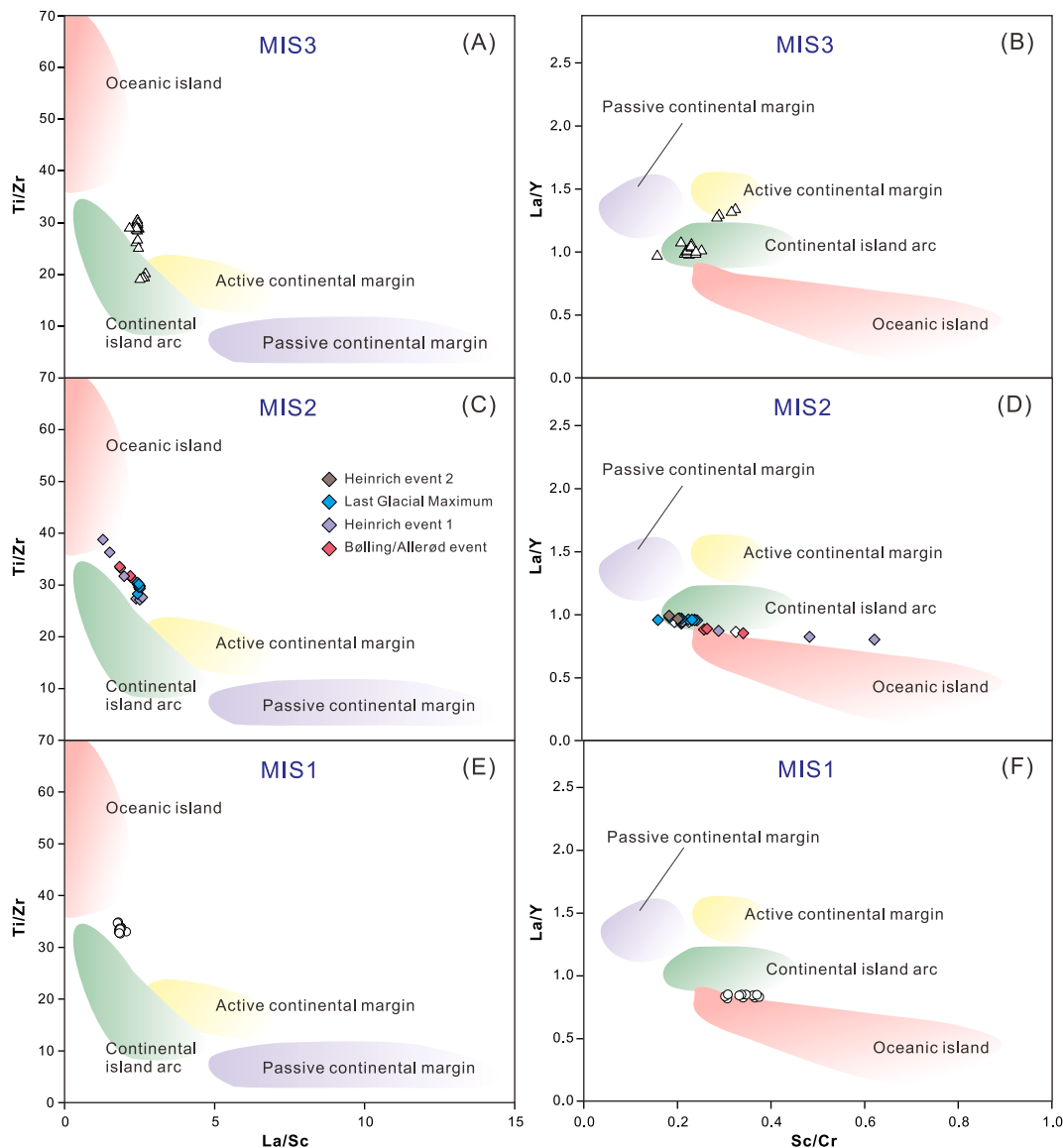


Fig. 6. Discrimination plots showing the tectonic settings of sediments in different MIS (Roser and Korsch, 1988). The brown rhombus indicates the samples from Heinrich event 2. The blue rhombus indicates the samples from Last Glacial Maximum. The Purple rhombus indicates the samples from Heinrich event 1. The red rhombus indicates the samples from Bølling/Allerød event.

determine whether the sediments from distant land or local seamount before tracing the provenance.

Eu anomalies in chondrite-normalized REE patterns help to determine the parent rocks of sediments, as negative Eu anomalies instruct sedimentary rocks including sandstone, mudstone, carbonate rocks, and granite (Taylor and McLennan, 1985; Rollinson and Pease, 2021). Eu/Eu* values ranging from 0.79 to 0.89 among all samples in GT05 show slightly negative Eu anomalies, and both the chondrite-normalized and UCC-normalized patterns indicate the addition of terrigenous sediments (Fig. 2). Immobile trace elements are common indices for distinguishing rock types of sediments, owing to their stability during transport and deposition, as well as their ratios being more sensitive than elemental abundances (Rollinson and Pease, 2021). Ratios such as La/Sc, Co/Th, and La/Th contain key information indicating characteristics of parent rocks (McLennan et al., 1993). Samples in GT05 mainly exhibit a close relationship to acidic arc source with rock types between andesite and felsic volcanic rocks (Fig. 5).

Sediments derived from various parent rocks display diverse scenarios in trace element compositions due to different tectonic settings. Conversely, discrimination diagrams based on trace elements ratios

could be used to distinguish tectonic settings (Roser and Korsch, 1988; Armstrong-Altrin and Verma, 2005). All samples in this study can be divided into three main groups (MIS 1, MIS 2 and MIS 3) based on calibrated age model and observed variations across different stages (Fig. 6). During MIS 3, samples are predominantly associated with continental island arc, with some located near active continental margin (Fig. 6A-B). In MIS 2, corresponding to a relatively cold period that experienced several climate events including LGM, B/A, and Heinrich events, creating a more chaotic pattern. The results indicate that the samples in GT05 stabilized within continental island arc setting, until Heinrich event 1 (HE1) when they moved closer to oceanic island (Fig. 6C-D). In MIS 1, all samples are concentrated between continental island arc and oceanic island (Fig. 6E-F). In addition, we found our samples might be the mix of different types, which need to be focus that there might be sediments weathered from original seamount rocks according to the results.

5.2. Provenance of sediments

From trace elements analysis (Fig. 3), we found regular variations

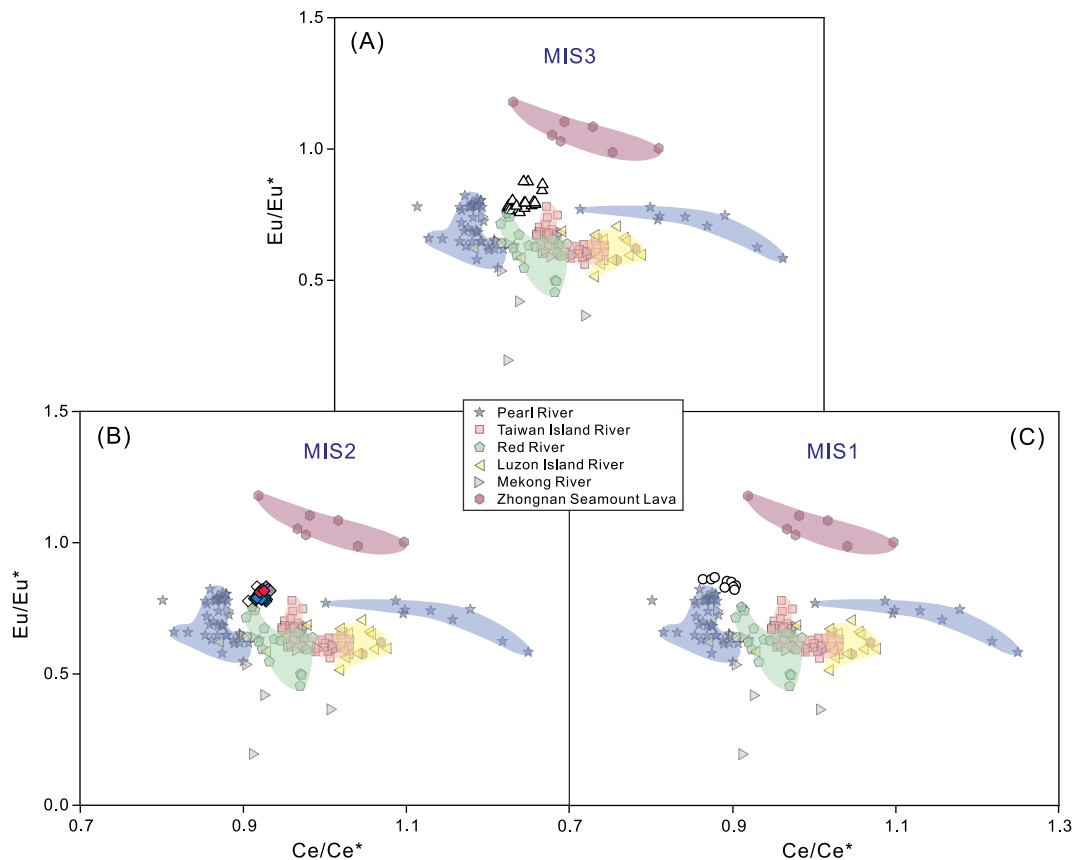


Fig. 7. Eu/Eu* vs. Ce/Ce* plots discriminating the relationship between sediments in the core GT05 and the surrounding sources. The data of Pearl River are from Xu and Han (2009); Taiwan Island River are from Li et al. (2013); Red River and Mekong River are from Borges et al. (2008); Luzon Island River are from DuFrane et al. (2006); Zhongnan Seamount Lava are from Qian et al. (2021). The sample legend is the same as Fig. 6.

with great match to climate events, however, there is no similar evidence for the clay minerals which shows a mess (Fig. 4), and we attribute the situation to a mix of different sources. Besides, when analyzing provenance of sediments, there is a scenario that might be easy to overlook. When sea level drop during glacial period, the continental shelf has become exposed land which originally deposit sediments from rivers, these regions could become the source and those sediments could be re-transported to further ocean. In this case, we collect data both from land and continental shelf to better uncover the provenance and transport pathway of sediments during different periods.

Eu and Ce anomalies could represent the condition of source rocks and environment (Taylor and McLennan, 1985), we collect data from source regions and compare the differences between our sediments and sources. In Fig. 7, the results show that sediments in GT05 are mixed by several sources, and Zhongnan Seamount Lava might have shown slight influence to the sediments. Combined with the results above (Figs. 4 and 5), sediments in GT05 show relationships with andesite and oceanic island, indicating a small part of sediments are derived from original seamount rocks. In MIS 3, samples mainly show similarities with Red River and Taiwan Island River (Fig. 7A). In MIS 2, samples are plotted closer to Red River but far away from Zhongnan Seamount Lava compared to MIS 3 (Fig. 7B). In MIS1, samples show close relationships with Pearl River (Fig. 7C).

Trace elements such as La, Th, and Sc are conservative during the sedimentary process and typically vary in source areas. Therefore, the La-Th-Sc discrimination diagram has become a useful tool to identify the provenance of sediments (Wei et al., 2012). The results show terrigenous sources mix with Zhongnan Seamount Lava, and indicate a certain degree of differentiation among all the sources, although some overlap is observed (Fig. 8). Notably, our findings reveal distinct patterns across

the three stages from MIS 3 to MIS 1. In MIS 3, samples mainly fall within the field between the northwestern and northern SCS (Fig. 8A). Compared to MIS 3, some samples in MIS 2 are plotted similarly, while others show the addition of sediments derived from northeast basin and offshore Luzon during HE1 (Fig. 8B). In MIS 1, there appears to be a shift in the provenance of samples, as they are much closer to the northeast basin and offshore Luzon Island after the B/A period (Fig. 8C). As shown from the above, we found some similarities showing same directions for our provenance analysis from different proxies. In MIS 3 and MIS 2, both the two diagrams indicate that Red River is the important sources of sediments in GT05.

The different results shown from the above have prevent our provenance analysis due to the similar trace element values of sources and limitation of single methods. Previous studies have extensively analyzed clay minerals in the SCS and surrounding source terrains, establishing this method as an efficient tool for tracing the source of sediments during the late Quaternary (Liu et al., 2004, 2010, 2016). However, the input of several sources and complex transport pathways has complicated the analysis, making it challenging to identify clear cycles (Boulay et al., 2005). Our results show that there is no obvious glacial-interglacial cyclicity from MIS 3 to MIS 1 (Fig. 4), indicating a mixture of different sources and complex variations during precipitation.

The results of clay minerals analysis suggest that these samples are closely related to the Red River and Taiwan Island during MIS 3 but also exhibit a distance from Taiwan Island during the LGM (Fig. 8A–B), which shows same variation as the result of trace elements (Fig. 7A–B). In addition, samples are plotted closer to Taiwan Island in HE1 and then move away until the B/A (Fig. 9B), which also show close relationship with Taiwan Island in trace element diagram (Fig. 7B). In MIS 1, the

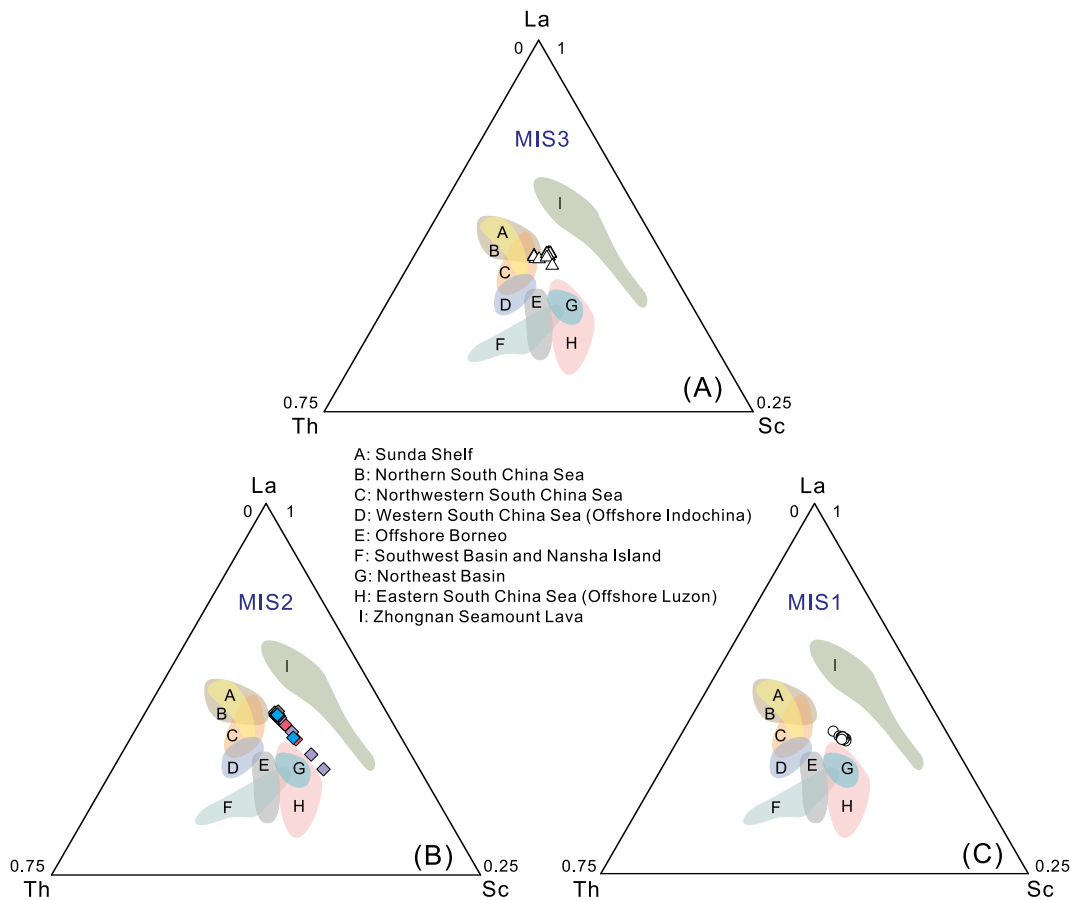


Fig. 8. La-Th-Sc ternary plots showing the relationship between sediments in the core GT05 and the SCS. The data of sediments in the SCS are collected from Wei et al. (2012) and Cao et al. (2019). The data of Zhongnan Seamount Lava are collected from Qian et al. (2021). The sample legend is the same as Fig. 6.

results show a mixed source from both Taiwan Island and the Red River (Fig. 9C). In addition, some samples in this study are tilted to the right and down due to the addition of smectite (Fig. 9). Smectite originates from the removal of mobile ions from minerals, which has found enrichment of smectite in Luzon, identifying it as a primary source of smectite in the northern SCS (Liu et al., 2016). The presence of smectite in our results may be attributed to sediment input from Luzon since MIS 2 (Fig. 9B).

Besides, compared to clay minerals in the SCS, samples are plotted mainly in northeastern SCS, gulf of Tonkin and northwestern SCS in MIS 3 (Fig. 10A), the La-Th-Sc diagram shows a same result that samples are close to northwestern SCS (Fig. 8A). In MIS 2, northeastern SCS samples decrease but northwestern SCS increase, especially in LGM, however, samples are plotted closer to northeastern SCS in HE1 and then move away until the B/A (Fig. 10B), the La-Th-Sc diagram shows the relationship that samples are plotted closer to northeast basin in HE1 but move away in the B/A (Fig. 8B). In MIS 3, samples are plotted both in northeastern SCS, gulf of Tonkin and northwestern SCS (Fig. 10C), however, result of trace elements shows close relationship with the northeast basin and offshore Luzon (Fig. 8C).

Although our provenance analysis shows a few differences between trace elements and clay minerals, there are important results in common which could reflect the same variations and help to decode the provenance. In summary, our results indicate that the source of sediments in Zhongnan Seamount varies across different sedimentary stages. During MIS 3, Taiwan Island and Red River were the primarily sources for the sediments, and the northwestern SCS also show close relationship. In LGM, the proportion of sediments from Taiwan Island decreases, while that the Red River-derived and Luzon Island-derived sediments increase, along with the northeastern SCS sediments decrease but northwestern

and eastern SCS increase. During HE1, the Taiwan Island-derived sediments increases but decrease after the B/A period, and the northeastern SCS also shows the same variation. In MIS 1, the provenance is dominantly from the islands of Taiwan Island and Red River, with addition contribution from the Luzon Island, sediments also show close relationship with the northeast basin and offshore Luzon.

5.3. Hydrodynamic patterns and transport pathways

5.3.1. MIS 3

Dry and cold climate conditions might have altered the land-sea interactions and ocean currents, affecting the transport of sediments from the land to open ocean. MIS 3 was a relatively weak glacial period, with the sea level below 60 m but falling to 100 m as the climate became colder (Miller et al., 2020). This decline in sea level led to the exposure and erosion of the continental shelf in the SCS. Consequently, drainage systems extended toward the edge of the shelf, facilitating erosion of sediments from the shelf and transport of sediments from rivers further into the ocean. Trace elements fluctuate greatly in this period, with nearly all values rising before HE3 and reaching their peak before HE2 (Fig. 3). Except for the abnormal variation at ca. 35 ka, clay minerals do not show sharp fluctuations until ca. 27 ka, suggests that the provenance is relatively steady during MIS 3 (Fig. 4). Provenance results suggest that Taiwan Island and the Red River are the primary sources during MIS 3 (Fig. 7A and 9A), importantly, sediments from northwestern SCS also show close relationship (Fig. 8A). Therefore, we propose that these variations might be linked to the extension of the Red River (Funabiki et al., 2007; Li et al., 2022; Tanabe et al., 2003; Wetzel et al., 2017). As a result, the input of sediments from Red River and the northwestern SCS to further SCS increased.

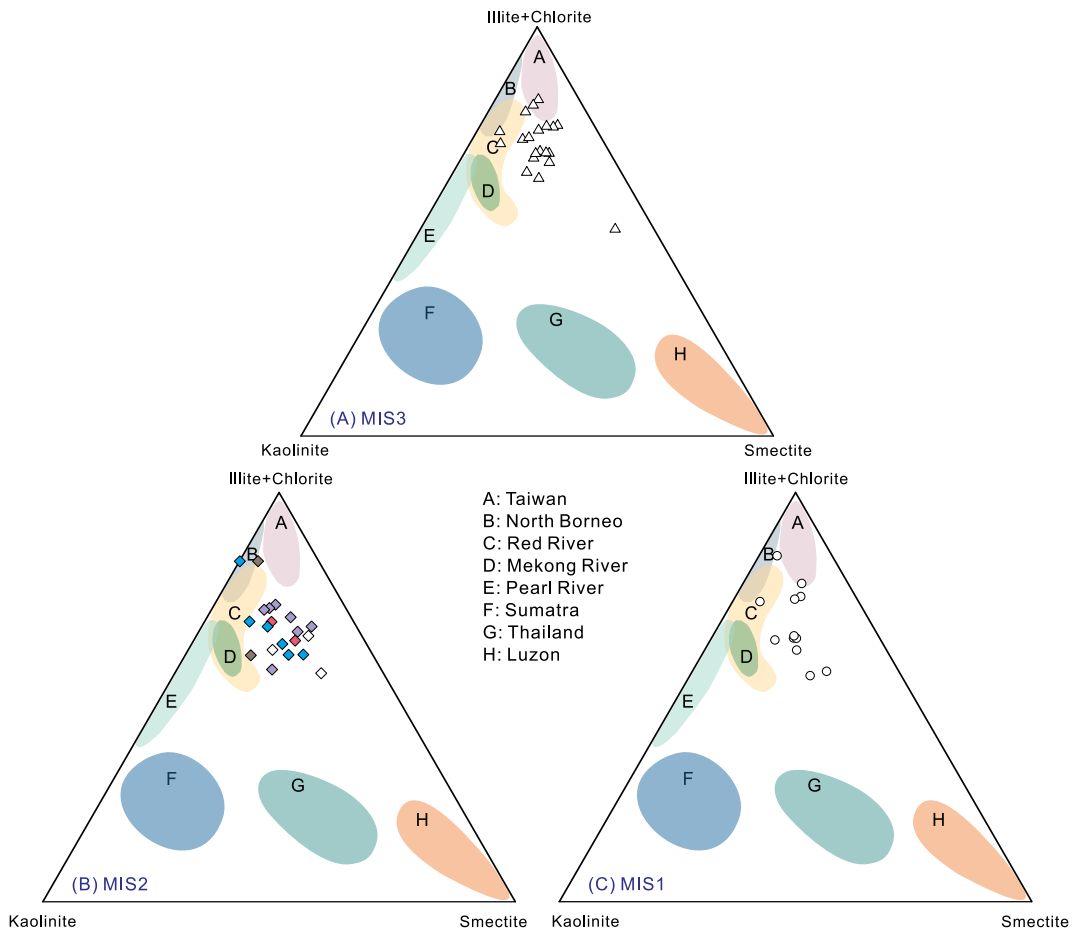


Fig. 9. (Illite + Chlorite)-Kaolinite-Smectite ternary plots of sediments in core GT05 and surrounding drainage systems, discriminating the sediment provenance from MIS 3 to MIS 1. The data of potential sources are from Liu et al. (2007, 2008c, 2010, 2012, 2016). The legend is the same as Fig. 6.

During MIS 3, the EAWM was stronger than it is today, resulting in the SCS being dominated by the strengthened surface currents in winter (Wang et al., 2001; Zhang et al., 2018), which in turn promoted the southward transport of sediments derived from the Red River. However, there may have been an intermedia or deep ocean current leading Red River-derived sediments southeastward to Zhongnan Seamount (Fig. 11A). Regarding the sediments from Taiwan Island, both the SCS Contour Current and deep ocean currents would have helped transport sediments to Zhongnan Seamount, except for the surface currents in winter (Fig. 11A).

5.3.2. MIS 2

Illite chemical index and crystallinity are useful for evaluating the weathering and climate conditions. The illite chemical index value below 0.5 indicates physical erosion, while above 0.5 suggests strong hydrolysis (Gingeletal., 1998). Our results show a relatively high illite chemical index values from the LGM to HE1 (Fig. 4). However, the intensified EAWM during glacial periods resulting in more physical denudation. This raises an enigmatic question: how did this situation happened under severe dry and cold climate condition?

Illite and chlorite are typically formed under conditions of weak hydrolysis or strong physical erosion, usually representing active tectonics and precipitation-caused physical erosion (Liu et al., 2016). The Red River region contains a high content of illite due to the relief of eastern Tibetan Plateau and Indochina Peninsula, and also exhibits a higher illite chemical index and stronger hydrolysis (Liu et al., 2007). Kaolinite is formed under warm and humid climate (Chamley, 1989), and it is enriched in the Pearl River and Red River (Liu et al., 2016). Zhang et al. (2023) indicated that both the Red River and Taiwan Island

were the major sources of fine-grained sediments in the Xisha Trough during the LGM. However, Taiwan Island gradually became the dominant supplier for the sediments in the MIS 1. Our provenance analysis indicates that Red River-derived and northwestern SCS sediments increased since the LGM (Fig. 7B, 9B and 10B), which may explain the abnormal increase in input from the Red River. The kaolinite/(illite + chlorite) values also correspond to the variations in the illite chemical index during the LGM, with an increase in kaolinite due to greater sediment input from the Red River (Fig. 4).

Under extremely dry and cold climate conditions, the sea level dropped to ca. 120 m, and the continental shelf in the SCS widely exposed during the LGM. On this occasion, the river systems have extended toward the shelf break zone (Zong et al., 2012; Sheng et al., 2024), and the ocean circulations altered greatly (Liu et al., 2016). Compared with MIS 3, the increased contribution of the Red River and northwestern SCS would have been due to the wide expanse of the river system, making its sediments much easier to input and transport (Fig. 11B). On the contrary, due to the typhoon rainfall-controlled sediment input and the narrow distance from river mouth to continental slopes, sediments from the islands of Taiwan Island and Luzon remains unaffected by the sea level changes during glacial-interglacial periods (Liu et al., 2009, 2010). Given that Luzon acts as the primary source of smectite, the smectite/(illite + chlorite) ratio has the potential to signify the transport capacity between surface and deep ocean currents in the northeastern SCS (Liu et al., 2010). Since the LGM, the North Pacific Intermediate Water (NPIW) has been enhanced and became the prominent source of deep water in the northeastern SCS (Wan and Jian, 2014; Wan et al., 2018). However, due to the higher temperature, lower salinity, and lighter density compared to the NPDW, the pressure

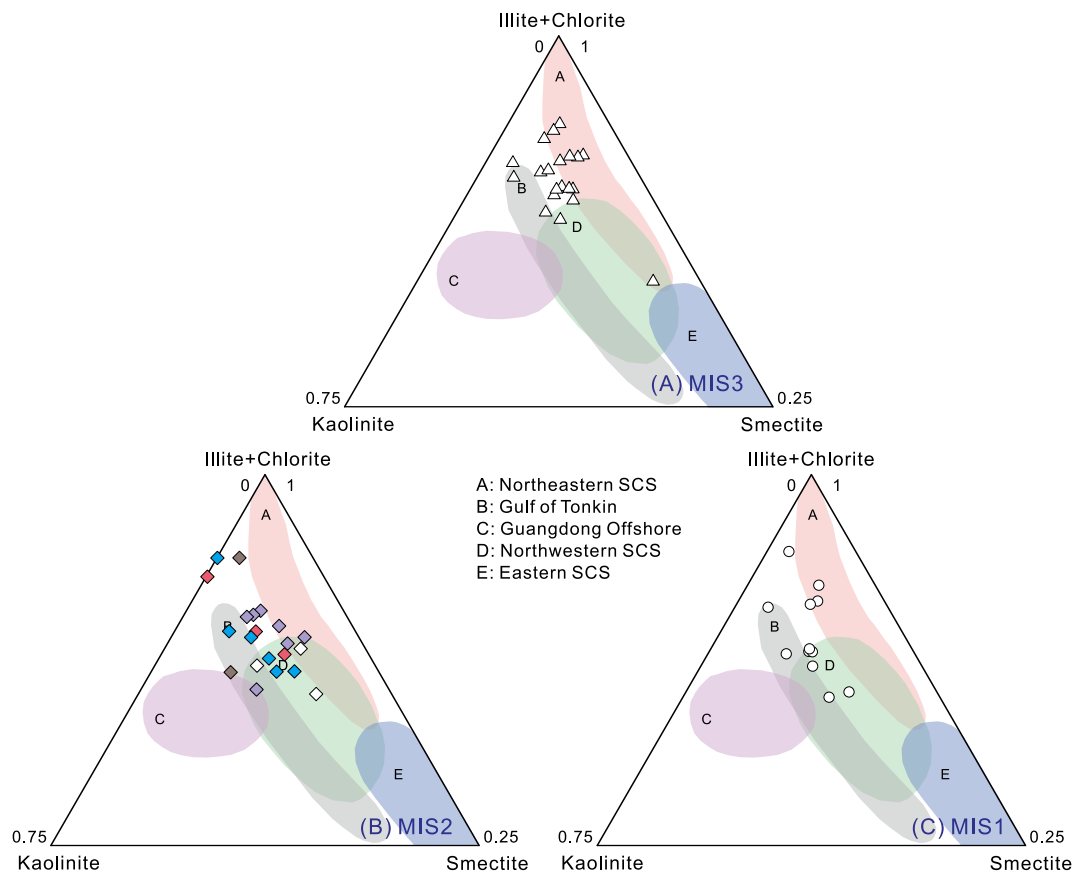


Fig. 10. (Illite + Chlorite)-Kaolinite-Smectite ternary plots of sediments in core GT05 and surrounding regions in SCS, discriminating the sediment provenance from MIS 3 to MIS 1. The data of potential sources are from Liu et al. (2007, 2008c, 2010, 2012, 2016). The legend is the same as Fig. 6.

gradient on both sides of the Luzon Strait has been decreased by NPIW, resulting in a slowing down of the deep circulation in the SCS (Zhao et al., 2023). Our smectite/(illite + chlorite) ratios have shown an increase since the LGM (Fig. 4). Combined with our provenance results, it might indicate a lower input of Taiwan Island-derived sediments transported by the deep ocean currents but an increase of Luzon-derived sediments by the surface currents.

Our study indicates that the high values of most elements during the LGM might be related to the increased input of the Red River, however, the rate dropped to lower values since HE1 (Fig. 11C). There is a sudden lowering of element ratios in the HE1 and a vertical elevation during the boundary between the HE1 and B/A (Fig. 3), which might have been related to severe climate change that could alter the input of sediments. Previous study found a reduction of Luzon-derived sediments during HE1 when analyzing the provenance of the northern slope of SCS, this situation is attributed to the southward shift of the summer Intertropical Convergence Zone (ITCZ) and the weaken of Kuroshio Current and upper currents (Liu et al., 2010). Our results also indicate a lower input of Luzon during the HE1 (Fig. 8B and 9B), with the decrease of smectite content (Fig. 4), which might be related to the southward shift of the ITCZ.

5.3.3. MIS 1

During MIS 1, samples exhibit a trend of stabilizing at comparatively lower element values (Fig. 3). Provenance results show a mixed source that derived from the Red River, Taiwan Island, Luzon Island, northeast Basin (Fig. 8C, 9C and 10C). During the interglacial period, the surface currents in summer are enhanced by the strong EASM (Wang et al., 2001; Zhang et al., 2018, 2020b). As a result, the northward surface currents in the western SCS prevent sediments from the Pearl River and Red River from transporting southward (Liu et al., 2016). However, our

results indicate that the sediment samples are still derived from the Red River, represents a small proportion from the northwestern SCS (Figs. 8C and 10C). In addition to the SCS Contour Current, the Luzon Deep Current has become another potential way to transport sediments from eastern Taiwan Island (Wang et al., 2022). In addition, the Kuroshio Current and Deep Cyclonic Current might also have been the important currents for sediments transporting from both Taiwan Island and Luzon Island to Zhongnan Seamount during interglacial period (Fig. 11D).

6. Conclusion

In this study, geochemistry and clay minerals are used to investigate the provenance of sediments from the Zhongnan Seamount in the central South China Sea, with aims to understand the source-to-sink process and transport dynamics within the seamount system. The sediments within the Zhongnan Seamount exhibit distant land-sourced characteristics, distinguished by specific geochemical signatures, including slight Eu anomalies (with Eu/Eu^* values ranging from 0.79 to 0.89) and compositions typical of andesitic/felsic igneous types. Our findings reveal a significant variation in provenance since MIS 3. Specifically, during MIS 3, the primary sediment provenance was identified as Taiwan Island and the Red River. However, during the LGM, Taiwan Island's contribution decreased while that of the Red River increased. Subsequently, in MIS 1, the main sources of sediment shifted to the islands of Taiwan Island and Luzon Island. The transport pathways of sediments and hydrodynamic patterns in the central South China Sea have undergone changes during different climatic stages, significantly influenced by the fluctuations in sea levels and shifts in monsoonal patterns. Consequently, there have been variations in sediment inputs from various sources. This study offers insights into how sediments within seamounts can potentially serve as records of hydrodynamic patterns, thereby revealing transport

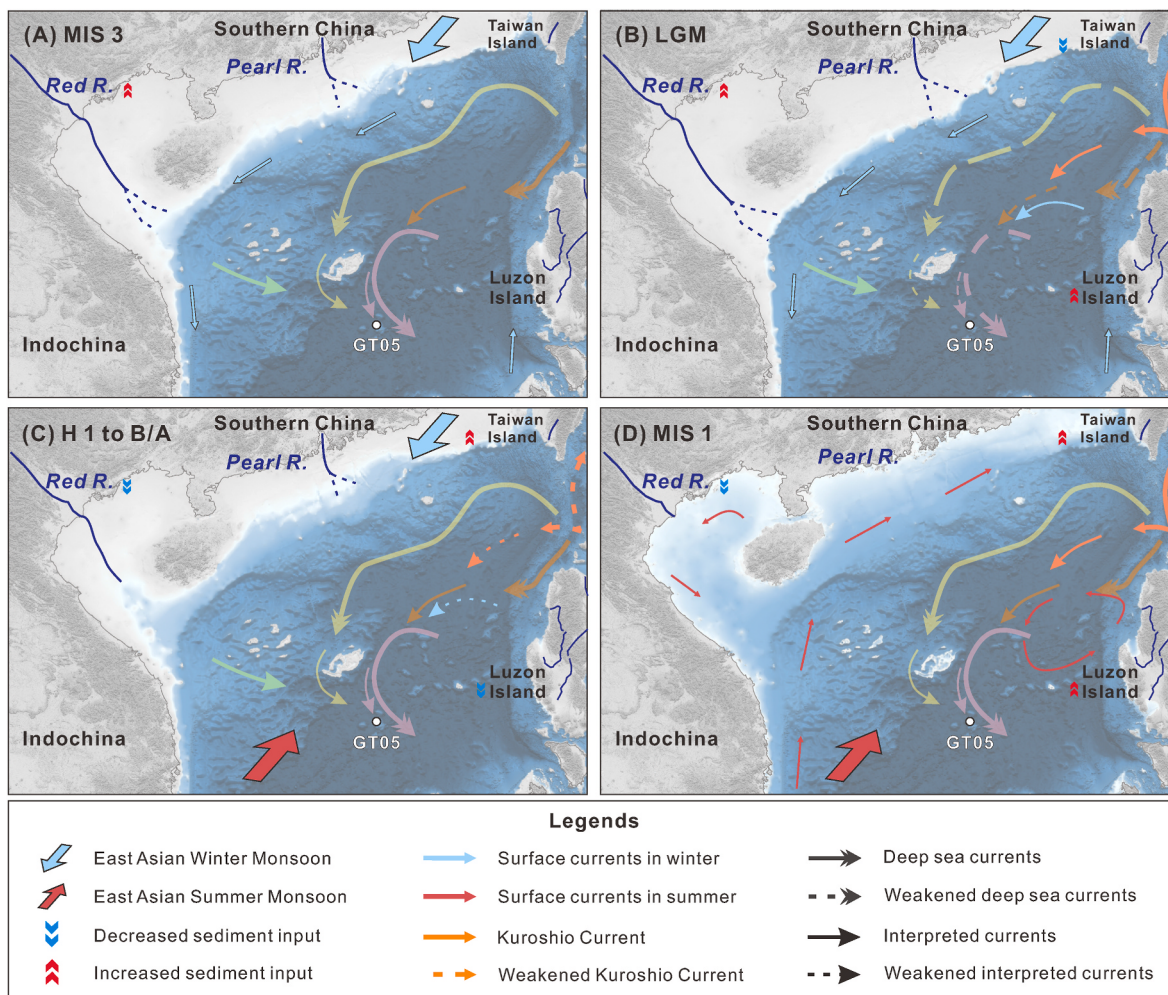


Fig. 11. Interpreted hydrodynamic model patterns illustrate the likely transport pathway from surrounding sources to core GT05 since MIS 3. The current systems have been simplified following the work of Wang et al. (1995). The extend of river systems are modified after Liu et al. (2016). (A) The coastline was moved to approximately present 100 m isobaths in MIS 3, and the drainage systems extended seaward; (B) The coastline was moved farthest to approximately present 120 m isobaths in the LGM, and drainage systems extended to the shelf break zone; (C) The coastline was moved back as the sea level rise due to the warming of climate since HE1, causing drainage systems to retreat toward land; (D) The coastline is similar to present day, as the sea level rise nearly same as present, no drainage systems extend seaward.

pathways within the seamount source-to-sink systems.

CRediT authorship contribution statement

Letian Zeng: Formal analysis, Investigation, Writing – original draft. Ce Wang: Methodology, Conceptualization, Project administration, Writing – review & editing. Ming Su: Methodology, Writing – review & editing. Heqi Cui: Investigation, Methodology.

Declaration of competing interest

The authors declare that they have no known competing financial interests or personal relationships that could have appeared to influence the work reported in this paper.

Acknowledgements

This work was supported by funding of the National Natural Science Foundation of China (No. 42172111), and the Innovation Group Project of Southern Marine Science and Engineering Guangdong Laboratory (Zhuhai) (No. 311022005). We gratefully acknowledge Cruise TS16, carried out by the R/V Tansuoyihao in the South China Sea in March

2020, for providing the sediment samples used in this study.

Appendix A. Supplementary data

Supplementary data to this article can be found online at <https://doi.org/10.1016/j.quascirev.2025.109585>.

Data availability

All data and/or code is contained within the submission.

References

- Armstrong-Altrin, J.S., Verma, S.P., 2005. Critical evaluation of six tectonic setting discrimination diagrams using geochemical data of Neogene sediments from known tectonic settings. *Sediment. Geol.* 177, 115–129. <https://doi.org/10.1016/j.sedgeo.2005.02.004>.
- Biscaye, P.E., 1965. Mineralogy and sedimentation of recent deep-sea clay in the Atlantic Ocean and adjacent seas and oceans. *Geol. Soc. Am. Bull.* 76, 803–832. [https://doi.org/10.1130/0016-7606\(1965\)76\[803:MASORD\]2.0.CO;2](https://doi.org/10.1130/0016-7606(1965)76[803:MASORD]2.0.CO;2).
- Borges, J.B., Huh, Y., Moon, S., Noh, H., 2008. Provenance and weathering control on river bed sediments of the eastern Tibetan Plateau and the Russian Far East. *Chem. Geol.* 254, 52–72. <https://doi.org/10.1016/j.chemgeo.2008.06.002>.
- Boulay, S., Colin, C., Trentesaux, A., Frank, N., Liu, Z., 2005. Sediment sources and East Asian monsoon intensity over the last 450 ky. Mineralogical and geochemical

- investigations on South China Sea sediments. *Palaeogeogr. Palaeoclimatol. Palaeoecol.* 228, 260–277. <https://doi.org/10.1016/j.palaeo.2005.06.005>.
- Briais, A., Patriat, P., Tappognon, P., 1993. Updated interpretation of magnetic anomalies and seafloor spreading stages in the south China Sea: implications for the Tertiary tectonics of Southeast Asia. *J. Geophys. Res. Solid Earth* 98, 6299–6328. <https://doi.org/10.1029/92jb02280>.
- Broecker, W., Clark, E., Barker, S., 2008. Near constancy of the Pacific Ocean surface to mid-depth radiocarbon-age difference over the last 20 kyr. *Earth Planet Sci. Lett.* 274, 322–326. <https://doi.org/10.1016/j.epsl.2008.07.035>.
- Cao, L., Liu, J., Shi, X., He, W., Chen, Z., 2019. Source-to-sink processes of fluvial sediments in the northern South China Sea: constraints from river sediments in the coastal region of South China. *J. Asian Earth Sci.* 185, 104020. <https://doi.org/10.1016/j.jseas.2019.104020>.
- Caruso, M.J., Gawarkiewicz, G.G., Beardsley, R.C., 2006. Interannual variability of the Kuroshio intrusion in the South China sea. *J. Oceanogr.* 62, 559–575. <https://doi.org/10.1007/s10872-006-0076-0>.
- Chamley, H., 1989. *Clay Sedimentology*. Springer Science & Business Media.
- Chen, Q., Liu, Z., Kissel, C., 2017. Clay mineralogical and geochemical proxies of the East Asian summer monsoon evolution in the South China sea during late quaternary. *Sci. Rep.* 7, 42083. <https://doi.org/10.1038/srep42083>.
- Chen, J., Zou, J., Zhu, A., Shi, X., Nürnberg, D., Lembeke-Jene, L., Tiedemann, R., Wang, K., Wu, Y., Dong, Z., Liu, J., Dou, R., 2021. Geochemistry of surface sediments from the emperor seamount chain, North Pacific. *Front. Earth Sci.* 9, 674842. <https://doi.org/10.3389/feart.2021.674842>.
- Clark, M.R., Rowden, A.A., Schlacher, T., Williams, A., Consalvey, M., Stocks, K.I., Rogers, A.D., O'Hara, T.D., White, M., Shank, T.M., Hall-Spencer, J.M., 2010. The ecology of seamounts: structure, function, and human impacts. *Ann. Rev. Mar. Sci.* 2, 253–278. <https://doi.org/10.1146/annurev-marine-120308-081109>.
- Clift, P.D., 2016. Assessing effective provenance methods for fluvial sediment in the South China Sea. *Geol. Soc. Lond. Spec. Publ.* 429, 9–29. <https://doi.org/10.1144/sp429.3>.
- Ding, W., Li, J., Clift, P.D., 2016. Spreading dynamics and sedimentary process of the southwest sub-basin, south China sea: constraints from multi-channel seismic data and IODP expedition 349. *J. Asian Earth Sci.* 115, 97–113. <https://doi.org/10.1016/j.jseas.2015.09.013>.
- DuFrane, S.A., Asmerom, Y., Mukasa, S.B., Morris, J.D., Dreyer, B.M., 2006. Subduction and melting processes inferred from U-Series, Sr-Nd-Pb isotope, and trace element data, Bicol and Bataan arcs, Philippines. *Geochem. Cosmochim. Acta* 70, 3401–3420. <https://doi.org/10.1016/j.gca.2006.04.020>.
- Ehrmann, W., 1998. Implications of late Eocene to early Miocene clay mineral assemblages in McMurdo Sound (Ross Sea, Antarctica) on paleoclimate and ice dynamics. *Palaeogeogr. Palaeoclimatol. Palaeoecol.* 139, 213–231. [https://doi.org/10.1016/S0031-0182\(97\)00138-7](https://doi.org/10.1016/S0031-0182(97)00138-7).
- Floyd, P., Leveridge, B., 1987. Tectonic environment of the Devonian Gramscatho basin, south Cornwall: framework mode and geochemical evidence from turbiditic sandstones. *J. Geol. Soc.* 144, 531–542. <https://doi.org/10.1144/gjs.144.4.0531>.
- Funabiki, A., Haruyama, S., Quy, N. Van, Hai, P. Van, Thai, D.H., 2007. Holocene delta plain development in the Song Hong (Red River) delta, Vietnam. *J. Asian Earth Sci.* 30, 518–529. <https://doi.org/10.1016/j.jseas.2006.11.013>.
- Gan, J., Li, H., Curchitser, E.N., Haidvogel, D.B., 2006. Modeling South China Sea circulation: response to seasonal forcing regimes. *J. Geophys. Res.* 111, C06034. <https://doi.org/10.1029/2005jc003298>.
- Ginge, F., Müller, P., Schneider, R., 1998. Orbital forcing of freshwater input in the Zaire Fan area—clay mineral evidence from the last 200 kyr. *Palaeogeogr. Palaeoclimatol. Palaeoecol.* 138, 17–26. [https://doi.org/10.1016/S0031-0182\(97\)00121-1](https://doi.org/10.1016/S0031-0182(97)00121-1).
- Hay, W.W., 1998. Detrital sediment fluxes from continents to oceans. *Chem. Geol.* 145, 287–323. [https://doi.org/10.1016/S0009-2541\(97\)00149-6](https://doi.org/10.1016/S0009-2541(97)00149-6).
- Hu, J., Kawamura, H., Hong, H., Qi, Y., 2000. A review on the currents in the South China Sea: seasonal circulation, South China Sea warm current and Kuroshio intrusion. *J. Oceanogr.* 56, 607–624. <https://doi.org/10.1023/A:1011117531252>.
- Hu, D., Böning, P., Köhler, C.M., Hillier, S., Pressling, N., Wan, S., Brumsack, H.J., Clift, P.D., 2012. Deep sea records of the continental weathering and erosion response to East Asian monsoon intensification since 14ka in the South China Sea. *Chem. Geol.* 326–327, 1–18. <https://doi.org/10.1016/j.chemgeo.2012.07.024>.
- Huang, R., Zhou, L., Chen, W., 2003. The progresses of recent studies on the variabilities of the East Asian monsoon and their causes. *Adv. Atmos. Sci.* 20, 55–69. <https://doi.org/10.1007/BF03342050>.
- Huang, R., Chen, J., Wang, L., Lin, Z., 2012. Characteristics, processes, and causes of the spatio-temporal variabilities of the East Asian monsoon system. *Adv. Atmos. Sci.* 29, 910–942. <https://doi.org/10.1007/s00376-012-2015-x>.
- Huang, C., Wang, P., Yu, M., You, C., Liu, C., Zhao, X., Shao, L., Zhong, G., Yumul, G., 2019. Potential role of strike-slip faults in opening up the South China Sea. *Natl. Sci. Rev.* 6, 891–901. <https://doi.org/10.1093/nsr/nwz119>.
- Huang, J., Jiao, W., Liu, J., Wan, S., Xiong, Z., Zhang, J., Yang, Z., Li, A., Li, T., 2021. Sediment distribution and dispersal in the southern South China Sea: evidence from clay minerals and magnetic properties. *Mar. Geol.* 439, 106560. <https://doi.org/10.1016/j.margeo.2021.106560>.
- Isobe, A., Namba, T., 2001. The circulation in the upper and intermediate layers of the South China sea. *J. Oceanogr.* 57, 93–104. <https://doi.org/10.1023/A:1011130905369>.
- Jian, Z., Huang, B., Kuhnt, W., Lin, H.L., 2001. Late quaternary upwelling intensity and east Asian monsoon forcing in the South China Sea. *Quat. Res.* 55, 363–370. <https://doi.org/10.1006/qres.2001.2231>.
- Jiang, X., Dong, C., Ji, Y., Wang, C., Shu, Y., Liu, L., Ji, J., 2021. Influences of deep-water seamounts on the hydrodynamic environment in the northwestern Pacific Ocean. *J. Geophys. Res. Oceans* 126, e2021JC017396. <https://doi.org/10.1029/2021JC017396>.
- Lambeck, K., Rouby, H., Purcell, A., Sun, Y., Cambridge, M., 2014. Sea level and global ice volumes from the last glacial maximum to the Holocene. *Proc. Natl. Acad. Sci. USA* 111, 15296–15303. <https://doi.org/10.1073/pnas.1411762111>.
- Lan, J., Zhang, N., Wang, Y., 2013. On the dynamics of the South China Sea deep circulation. *J. Geophys. Res. Oceans* 118, 1206–1210. <https://doi.org/10.1002/jgrc.20104>.
- Lavelle, J.W., Mohn, C., 2010. Motion, commotion, and biophysical connections at deep ocean seamounts. *Oceanography (Wash. D. C.)* 23, 90–103. <https://doi.org/10.5670/oceanog.2010.64>.
- Li, C.S., Shi, X.F., Kao, S.J., Liu, Y.G., Lyu, H.H., Zou, J.J., Liu, S.F., Qiao, S.Q., 2013. Rare earth elements in fine-grained sediments of major rivers from the high-standing island of Taiwan. *J. Asian Earth Sci.* 69, 39–47. <https://doi.org/10.1016/j.jseas.2013.03.001>.
- Li, C., Lin, J., Kulhanek, D., Williams, T., Bao, R., Braias, A., Brown, E., Chen, Y., Clift, P., Colwell, F., Dadd, K., Ding, W., Almeida, I., Huang, X., Hyun, S., Jiang, T., Koppers, A., Li, Q., Liu, C., Liu, Q., Liu, Z., Nagai, R., Peleo-Alampay, A., Su, X., Zhen, S., Tejada, M., Trinh, H., Yeh, Y., Zhang, C., Zhang, F., Zhang, G., Zhao, X., Tang, H., 2014. Opening of the South China Sea and its implications for southeast Asian tectonics, climates, and deep mantle processes since the late Mesozoic. *Integrated Ocean Drilling Program. Preliminary Reports* 349, 1–109. <https://doi.org/10.14379/iodp.pr.349.2014>.
- Li, Z., Lau, W.K.M., Ramamathan, V., Wu, G., Ding, Y., Manoj, M.G., Liu, J., Qian, Y., Li, J., Zhou, T., Fan, J., Rosenfeld, D., Ming, Y., Wang, Y., Huang, J., Wang, B., Xu, X., Lee, S.S., Cribb, M., Zhang, F., Yang, X., Zhao, C., Takemura, T., Wang, K., Xia, X., Yin, Y., Zhang, H., Guo, J., Zhai, P.M., Sugimoto, N., Babu, S.S., Brasseur, G. P., 2016. Aerosol and monsoon climate interactions over Asia. *Rev. Geophys.* 54, 866–929. <https://doi.org/10.1002/2015rg000500>.
- Li, M., Ouyang, T., Zhu, Z., Tian, C., Peng, S., Zhong, H., Peng, X., Qiu, Y., 2022. Reconstruction of chemical weathering intensity and Asian summer monsoon evolution in the Red River basin over the past 36 kyr. *Paleoceanogr. Paleoclimatol.* 37, e2021PA004397. <https://doi.org/10.1029/2021PA004397>.
- Liu, Z., Stattegger, K., 2014. South China Sea fluvial sediments: an introduction. *J. Asian Earth Sci.* 79, 507–508. <https://doi.org/10.1016/j.jseas.2013.11.003>.
- Liu, Z., Colin, C., Trentesaux, A., Blamart, D., Bassinot, F., Siani, G., Sicre, M.-A., 2004. Erosional history of the eastern Tibetan Plateau since 190 kyr ago: clay mineralogical and geochemical investigations from the southwestern South China Sea. *Mar. Geol.* 209, 1–18. <https://doi.org/10.1016/j.margeo.2004.06.004>.
- Liu, Z., Zhao, Y., Li, J., Colin, C., 2007. Late quaternary clay minerals off middle Vietnam in the western south China sea: implications for source analysis and East Asian monsoon evolution. *Sci. China Earth Sci.* 50, 1674–1684. <https://doi.org/10.1007/s11430-007-0115-8>.
- Liu, Q., Kaneko, A., Jian, S., 2008a. Recent progress in studies of the South China Sea circulation. *J. Oceanogr.* 64, 753–762. <https://doi.org/10.1007/s10872-008-0063-8>.
- Liu, Y., Zong, K., Kelemen, P.B., Gao, S., 2008b. Geochemistry and magmatic history of eclogites and ultramafic rocks from the Chinese continental scientific drill hole: subduction and ultrahigh-pressure metamorphism of lower crustal cumulates. *Chem. Geol.* 247, 133–153. <https://doi.org/10.1016/j.chemgeo.2007.10.016>.
- Liu, Z., Tuo, S., Colin, C., Liu, J.T., Huang, C.-Y., Selvaraj, K., Chen, C.-T.A., Zhao, Y., Siringan, F.P., Boulay, S., Chen, Z., 2008c. Detrital fine-grained sediment contribution from Taiwan Island to the northern South China Sea and its relation to regional ocean circulation. *Mar. Geol.* 255, 149–155. <https://doi.org/10.1016/j.margeo.2008.08.003>.
- Liu, Z., Zhao, Y., Colin, C., Siringan, F.P., Wu, Q., 2009. Chemical weathering in Luzon, Philippines from clay mineralogy and major-element geochemistry of river sediments. *Appl. Geochem.* 24, 2195–2205. <https://doi.org/10.1016/j.apgeochem.2009.09.025>.
- Liu, Z., Li, X., Colin, C., Ge, H., 2010. A high-resolution clay mineralogical record in the northern South China Sea since the Last Glacial Maximum, and its time series provenance analysis. *Chin. Sci. Bull.* 55, 4058–4068. <https://doi.org/10.1007/s11434-010-4149-5>.
- Liu, Z., Wang, H., Hantoro, W.S., Sathiamurthy, E., Colin, C., Zhao, Y., Li, J., 2012. Climatic and tectonic controls on chemical weathering in tropical southeast Asia (Malay Peninsula, Borneo, and Sumatra). *Chem. Geol.* 291, 1–12. <https://doi.org/10.1016/j.chemgeo.2011.11.015>.
- Liu, Z., Zhao, Y., Colin, C., Siringan, F.P., Wu, Q., 2009. Chemical weathering in Luzon, Philippines from clay mineralogy and major-element geochemistry of river sediments. *Appl. Geochem.* 24, 2195–2205. <https://doi.org/10.1016/j.apgeochem.2009.09.025>.
- McClain, C.R., 2007. Seamounts: identity crisis or split personality? *J. Biogeogr.* 34, 2001–2008. <https://doi.org/10.1111/j.1365-2699.2007.01783.x>.
- McLennan, S., Hemming, S., McDaniel, D., Hanson, G., 1993. Geochemical approaches to sedimentation, provenance, and tectonics. *Geol. Soc. Am. Bull.* 284, 21. <https://doi.org/10.1130/SPE284-p21>.
- Miller, K.G., Browning, J.V., Schmelz, W.J., Kopp, R.E., Mountain, G.S., Wright, J.D., 2020. Cenozoic sea-level and cryospheric evolution from deep-sea geochemical and continental margin records. *Sci. Adv.* 6, eaaz1346. <https://doi.org/10.1126/sciadv.aaz1346>.
- Milliman, J.D., Farnsworth, K.L., 2011. River Discharge to the Coastal Ocean: A Global Synthesis. Cambridge University Press, Cambridge, pp. 1–164. <https://doi.org/10.1017/CBO9780511781247>.

- Nan, F., Xue, H., Chai, F., Shi, L., Shi, M., Guo, P., 2011. Identification of different types of Kuroshio intrusion into the South China sea. *Ocean Dyn.* 61, 1291–1304. <https://doi.org/10.1007/s10236-011-0426-3>.
- Nan, F., Xue, H., Yu, F., 2015. Kuroshio intrusion into the South China sea: a review. *Prog. Oceanogr.* 137, 314–333. <https://doi.org/10.1016/j.pocean.2014.05.012>.
- Qian, S., Gazel, E., Nichols, A.R.L., Cheng, H., Zhang, L., Salters, V.J., Li, J., Xia, X., Zhou, H., 2021. The origin of late cenozoic magmatism in the South China sea and southeast Asia. *Geochemistry, Geophys. Geosystems* 22, 1–23. <https://doi.org/10.1029/2021GC009686>.
- Qu, T., Girton, J.B., Whitehead, J.A., 2006. Deepwater overflow through Luzon Strait. *J. Geophys. Res.* 111. <https://doi.org/10.1029/2005jc003139>.
- Rollinson, H., Pease, V., 2021. Using Geochemical Data: to Understand Geological Processes, 2 ed. Cambridge University Press, Cambridge. <https://doi.org/10.1017/9781108777834>.
- Roser, B.P., Korsch, R.J., 1988. Provenance signatures of sandstone–mudstone suites determined using discriminant function analysis of major-element data. *Chem. Geol.* 67, 119–139. [https://doi.org/10.1016/0009-2541\(88\)90010-1](https://doi.org/10.1016/0009-2541(88)90010-1).
- Rudnick, R.L., Gao, S., 2003. Composition of the Continental Crust. Treatise on Geochemistry. Pergamon, Oxford, pp. 1–64. <https://doi.org/10.1016/B0-08-043751-6/03016-4>.
- Sheng, C., Jiao, J., Zhang, J., Yao, Y., Luo, X., Yu, S., Ni, Y., Wang, S., Mao, R., Yang, T., Zhan, L., 2024. Evolution of groundwater system in the Pearl River Delta and its adjacent shelf since the late Pleistocene. *Sci. Adv.* 10, eadn3924. <https://doi.org/10.1126/sciadv.adn3924>.
- Sibuet, J.-C., Yeh, Y.-C., Lee, C.-S., 2016. Geodynamics of the South China sea. *Tectonophysics* 692, 98–119. <https://doi.org/10.1016/j.tecto.2016.02.022>.
- Staudigel, H., Koppers, A.A.P., 2015. Seamounts and island building. In: The Encyclopedia of Volcanoes. Elsevier Inc, pp. 405–421. <https://doi.org/10.1016/B978-0-12-385938-9.00022-5>.
- Sun, S.-S., McDonough, W.F., 1989. Chemical and isotopic systematics of oceanic basalts: implications for mantle composition and processes. *Geol. Soc. Lond. Spec. Publ.* 42, 313–345. <https://doi.org/10.1144/GSL.SP.1989.042.01.19>.
- Sun, Y., Chen, J., Clemens, S.C., Liu, Q., Ji, J., Tada, R., 2006. East Asian monsoon variability over the last seven glacial cycles recorded by a loess sequence from the northwestern Chinese Loess Plateau. *Geochem. Geophys. Geosyst.* 7, Q12Q02. <https://doi.org/10.1029/2006gc001287>.
- Tamburini, F., Adatte, T., Föllmi, K., Bernasconi, S.M., Steinmann, P., 2003. Investigating the history of East Asian monsoon and climate during the last glacial–interglacial period (0–140 000 years): mineralogy and geochemistry of ODP Sites 1143 and 1144, South China Sea. *Mar. Geol.* 201, 147–168. [https://doi.org/10.1016/s0025-3227\(03\)00214-7](https://doi.org/10.1016/s0025-3227(03)00214-7).
- Tanabe, S., Hori, K., Saito, Y., Haruyama, S., Vu, V.P., Kitamura, A., 2003. Song Hong (Red River) delta evolution related to millennium-scale Holocene sea-level changes. *Quat. Sci. Rev.* 22, 2345–2361. [https://doi.org/10.1016/S0277-3791\(03\)00138-0](https://doi.org/10.1016/S0277-3791(03)00138-0).
- Taylor, B., Hayes, D.E., 1980. The tectonic evolution of the South China Basin. *Geophys. Monogr. Ser.* 23, 89–104. <https://doi.org/10.1029/GM023p0089>.
- Taylor, B., Hayes, D.E., 1983. Origin and history of the South China sea basin. *Geophys. Monogr. Ser.* 27, 23–56. <https://doi.org/10.1029/GM027p0023>.
- Taylor, S.R., McLennan, S.M., 1985. The Continental Crust: its Composition and Evolution. Oxford Press, Blackwell, pp. 1–312.
- Turner, R., Falahat, S., Nycander, J., Dale, A., Scott, R.B., Furnival, D., 2013. Deep-sea fluid and sediment dynamics—fluence of hill- to seamount-scale seafloor topography. *Earth Sci. Rev.* 127, 203–241. <https://doi.org/10.1016/j.earscirev.2013.10.005>.
- Wan, S., Jian, Z., 2014. Deep water exchanges between the South China Sea and the Pacific since the last glacial period. *Paleoceanography* 29, 1162–1178. <https://doi.org/10.1002/2013pa002578>.
- Wan, S., Jian, Z., Dang, H., 2018. Deep hydrography of the South China sea and deep water circulation in the pacific since the last glacial maximum. *Geochem. Geophys. Geosyst.* 19, 1447–1463. <https://doi.org/10.1029/2017gc007377>.
- Wang, P., Sun, X., 1994. Last glacial maximum in China: comparison between land and sea. *Catena* 23, 341–353. [https://doi.org/10.1016/0341-8162\(94\)90077-9](https://doi.org/10.1016/0341-8162(94)90077-9).
- Wang, P., Wang, L., Bian, Y., Jian, Z., 1995. Late Quaternary paleoceanography of the South China Sea: surface circulation and carbonate cycles. *Mar. Geol.* 127, 145–165. [https://doi.org/10.1016/0025-3227\(95\)00008-M](https://doi.org/10.1016/0025-3227(95)00008-M).
- Wang, L., Sarnthein, M., Erlenkeuser, H., Grimalt, J.O., Grootes, P., Heilig, S., Ivanova, E., Kienast, M., Pelejero, C., Pflaumann, U., 1999. East Asian monsoon climate during the Late Pleistocene: high-resolution sediment records from the south China Sea. *Mar. Geol.* 156, 245–284. [https://doi.org/10.1016/S0025-3227\(98\)00182-0](https://doi.org/10.1016/S0025-3227(98)00182-0).
- Wang, Y., Cheng, H., Edwards, R.L., An, J., Shen, C., Dorale, J.A., 2001. A high-resolution absolute-dated Late Pleistocene monsoon record from Hulu Cave, China. *Science* 294, 2345–2348. <https://doi.org/10.1126/science.1064618>.
- Wang, B., Chang, C.-P., Wang, Z., Hendon, H., 2006. The Asian winter monsoon. In: The Asian Monsoon. Springer Berlin Heidelberg, pp. 89–127.
- Wang, G., Xie, S.-P., Qu, T., Huang, R.X., 2011. Deep South China sea circulation. *Geophys. Res. Lett.* 38, L05601. <https://doi.org/10.1029/2010gl046626>.
- Wang, C., Cui, H., Zeng, L., Su, M., 2022. Provenance of sediments in the northern Manila Trench: an assessment from detrital zircon geochronology. *Sci. China Earth Sci.* 66, 41–53. <https://doi.org/10.1007/s11430-022-9976-5>.
- Wang, M., Zheng, Z., Zhou, Q., Jia, G., Wang, C., Chen, X., Yin, K., Yu, K., Wang, D., Naafs, B.D.A., 2025. AMS ^{14}C Dating Results of Core GT05. Mendeley Data, V1. <https://doi.org/10.17632/y84f8x9bdg.1>.
- Webster, P.J., 1994. The role of hydrological processes in ocean-atmosphere interactions. *Rev. Geophys.* 32, 427–476. <https://doi.org/10.1029/94RG01873>.
- Wei, G., Liu, Y., Ma, J., Xie, L., Chen, J., Deng, W., Tang, S., 2012. Nd, Sr isotopes and elemental geochemistry of surface sediments from the South China Sea: implications for Provenance Tracing. *Mar. Geol.* 319–322, 21–34. <https://doi.org/10.1016/j.margeo.2012.05.007>.
- Wetzel, A., Szczygierski, A., Unverricht, D., Stattegger, K., 2017. Sedimentological and ichnological implications of rapid Holocene flooding of a gently sloping mud-dominated incised valley – an example from the Red River (Gulf of Tonkin). *Sedimentology* 64, 1173–1202. <https://doi.org/10.1111/sed.12357>.
- Wronkiewicz, D.J., Condie, K.C., 1987. Geochemistry of Archean shales from the Witwatersrand supergroup, South Africa: source-area weathering and provenance. *Geochim. Cosmochim. Acta* 51, 2401–2416. [https://doi.org/10.1016/0016-7037\(87\)90293-6](https://doi.org/10.1016/0016-7037(87)90293-6).
- Wu, D., Wang, Y., Lin, X., Yang, J., 2008. On the mechanism of the cyclonic circulation in the Gulf of Tonkin in the summer. *J. Geophys. Res.* 113, C09029. <https://doi.org/10.1029/2007jc004208>.
- Xu, Z., Han, G., 2009. Rare earth elements (REE) of dissolved and suspended loads in the Xijiang River, South China. *Appl. Geochem.* 24, 1803–1816. <https://doi.org/10.1016/j.apgeochem.2009.06.001>.
- Yan, Q., Shi, X., Wang, K., Bu, W., Xiao, L., 2008. Major element, trace element, and Sr, Nd and Pb isotope studies of Cenozoic basalts from the South China Sea. *Sci. China Ser D Earth Sci.* 51, 550–566. <https://doi.org/10.1007/s11430-008-0026-3>.
- Yan, Q., Shi, X., Castillo, P.R., 2014. The late Mesozoic–Cenozoic tectonic evolution of the South China Sea: a petrologic perspective. *J. Asian Earth Sci.* 85, 178–201. <https://doi.org/10.1016/j.jseas.2014.02.005>.
- Zhang, Y., Liu, Z., Zhao, Y., Wang, W., Li, J., Xu, J., 2014. Mesoscale eddies transport deep-sea sediments. *Sci. Rep.* 4, 5937. <https://doi.org/10.1038/srep05937>.
- Zhang, H., Griffiths, M.L., Chiang, J.C.H., Kong, W., Wu, S., Atwood, A., Huang, J., Cheng, H., Ning, Y., Xie, S., 2018. East Asian hydroclimate modulated by the position of the westerlies during Termination I. *Science* 362, 580–583. <https://doi.org/10.1126/science.aat9393>.
- Zhang, J., Li, J., Ruan, A., Ding, W., Niu, X., Wang, W., Tan, P., Wu, Z., Yu, Z., Wei, X., Zhao, Y., Zhou, Z., 2020a. Seismic structure of a postspreading seamount emplaced on the fossil spreading center in the southwest subbasin of the South China sea. *J. Geophys. Res. Solid Earth* 125, e2020JB019827. <https://doi.org/10.1029/2020JB019827>.
- Zhang, J., Lu, H., Jia, J., Li, F., 2020b. Seasonal drought events in tropical East Asia over the last 60,000 y. *Proc. Natl. Acad. Sci.* 117, 30988–30992. <https://doi.org/10.1073/pnas.2013802117>.
- Zhang, Q., Swann, G.E.A., Liu, J., Gao, W., Cui, Z., Li, G., Zhao, X., Li, W., 2023. Sea level controls on the provenance of fine-grained sediments in the Xisha Trough, northwestern South China Sea over the last ~30 ka. *Mar. Geol.* 466, 107184. <https://doi.org/10.1016/j.margeo.2023.107184>.
- Zhao, W., Zhou, C., Tian, J., Yang, Q., Wang, B., Xie, L., Qu, T., 2014. Deep water circulation in the Luzon Strait. *J. Geophys. Res. Oceans* 119, 790–804. <https://doi.org/10.1002/2013jc009587>.
- Zhao, Y., Wang, Y., Liu, Z., Li, X., Yang, W., 2023. Deep-water circulation intensity and stratification in the South China Sea since the last glaciation. *Mar. Geol.* 457, 107004. <https://doi.org/10.1016/j.margeo.2023.107004>.
- Zhong, Y., Chen, Z., Li, L., Liu, J., Li, G., Zheng, X., Wang, S., Mo, A., 2017. Bottom water hydrodynamic provinces and transport patterns of the northern South China Sea: evidence from grain size of the terrigenous sediments. *Cont. Shelf Res.* 140, 11–26. <https://doi.org/10.1016/j.csr.2017.01.023>.
- Zhu, Y., Sun, J., Wang, Y., Wei, Z., Yang, D., Qu, T., 2017. Effect of potential vorticity flux on the circulation in the South China Sea. *J. Geophys. Res. Oceans* 122, 6454–6469. <https://doi.org/10.1002/2016jc012375>.
- Zhu, Y., Sun, J., Wang, Y., Li, S., Xu, T., Wei, Z., Qu, T., 2019. Overview of the multi-layer circulation in the South China sea. *Prog. Oceanogr.* 175, 171–182. <https://doi.org/10.1016/j.pocean.2019.04.001>.
- Zong, Y., Huang, K., Yu, F., Zheng, Z., Switzer, A., Huang, G., Wang, N., Tang, M., 2012. The role of sea-level rise, monsoonal discharge and the palaeo-landscape in the early Holocene evolution of the Pearl River delta, southern China. *Quat. Sci. Rev.* 54, 77–88. <https://doi.org/10.1016/j.quascirev.2012.01.002>.